A Model for the Alboran Sea Internal Solitary Waves

STEFANO PIERINI

Istituto di Oceanologia, Istituto Universitario Navale, Napoli, Italy

(Manuscript received 20 May 1988, in final form 13 December 1988)

ABSTRACT

The propagation into the Alboran Sea of the interface depression generated at the Strait of Gibraltar by the interaction of the semidiurnal tidal current with the main (Camarinal) sill is studied numerically by using a unidirectional model with two horizontal space dimensions. An initial waveform within the strait is determined whose evolution corresponds with the train of internal solitary waves detected in the Alboran Sea by means of current measurements at different depths, as described by Kinder. The agreement is good for two points located at about 45 km east of the strait, the first aligned with the strait axis and the second 20 km to the north. Moreover, the shape and amplitude of this initial condition are in agreement with a typical interface depression generated in the strait by the interaction of the tidal current with the sill. A series of numerical experiments with different initial conditions is also performed to study the sensitivity of the model results to changes in the initial internal wave, and the reason why solitary waves may or may not be observed in the western part of the Alboran Sea is thus clarified. In general the horizontal shape of the waves is similar to that shown in pictures taken by the Space Shuttle *Challenger*. A discrepancy between the numerical and the observed shape, i.e., the higher curvature of the waves in a beam aligned with the strait axis, is to be accounted for by the advection due to the Atlantic water inflow which is not modeled here. The present study helps to understand the observed connection between the weakening of the Atlantic water jet (and corresponding weakening of the Alboran Sea gyre) and the appearance of energetic internal solitary waves.

1. Introduction

Internal waves horizontally propagating in the oceanic waveguide are nonlinear and dispersive. The degree of nonlinearity depends on the amplitude and length of the waves while phase dispersion is determined by their length relative to vertical length scales related to stratification and water depth. In general, for long waves these two dynamic effects tend to balance in such a way that nonperiodic, solitary waves emerge from an initially compact disturbance. In the oceans initial disturbances arising from the interaction between tidal currents and bathymetric features do give rise to propagating internal solitary waves. This is shown, for example, through CTD, XBT, current measurements and/or images from satellites and space shuttles in Massachusetts Bay (Lee and Beardsley 1974; Haury et al. 1979), in the Andaman Sea (Osborne and Burch 1980), in the New York Bight (Liu 1983), in the Tyrrhenian Sea (Alpers and Salusti 1983), in the Gulf of California (Fu and Holt 1984), in the Alboran Sea (Kinder 1984), in the Sulu Sea (Apel et al. 1985), etc.

As far as the modeling of nonlinear internal waves is concerned, in the case of straight-crested waves (one-dimensional) the Benjamin-Ono, the Kubota or the Korteweg-de Vries (KdV) equations apply according to whether the wavelength is much smaller, of the order of, or much larger than the water depth, respectively (see section 2). In most cases dealt with in the related literature the KdV equation is appropriate. For instance, in the papers quoted above KdV applies in all cases except for the Sulu Sea solitary waves. As far as the 1-D assumption is concerned, the only theoretical analysis in which 2-D spreading effects are taken into account appears to be that of Liu, A. K. et al. (1985) in which a generalized Kubota equation was used for the Sulu Sea waves.

The aim of this paper is to propose a model for the internal solitary waves detected in the Alboran Sea through current measurements (Kinder 1984) and visualized by images taken from the Space Shuttle *Challenger* (Fig. 1). Such waves are generated in the Strait of Gibraltar by the interaction of the semidiurnal tidal current with the main sill. They then propagate into the Alboran Sea with important spreading effects (Fig. 1). We will therefore make use of a 2-D evolution equation, the Kadomtsev–Petviashvili (1970, hereafter KP) equation, i.e, a 2-D generalization of the KdV equation, which we will solve using a finite-difference scheme (Pierini 1986).

We have determined an initial waveform inside the strait the evolution of which corresponds well with Kinder's data in two points in the Alboran Sea, where data are available. This will be discussed in section 4,

Corresponding author address: Dr. Stefano Pierini, Istituto di Oceanologia, Istituto Universitario Navale, Via Acton, 38, 80133 Napoli, Italy.

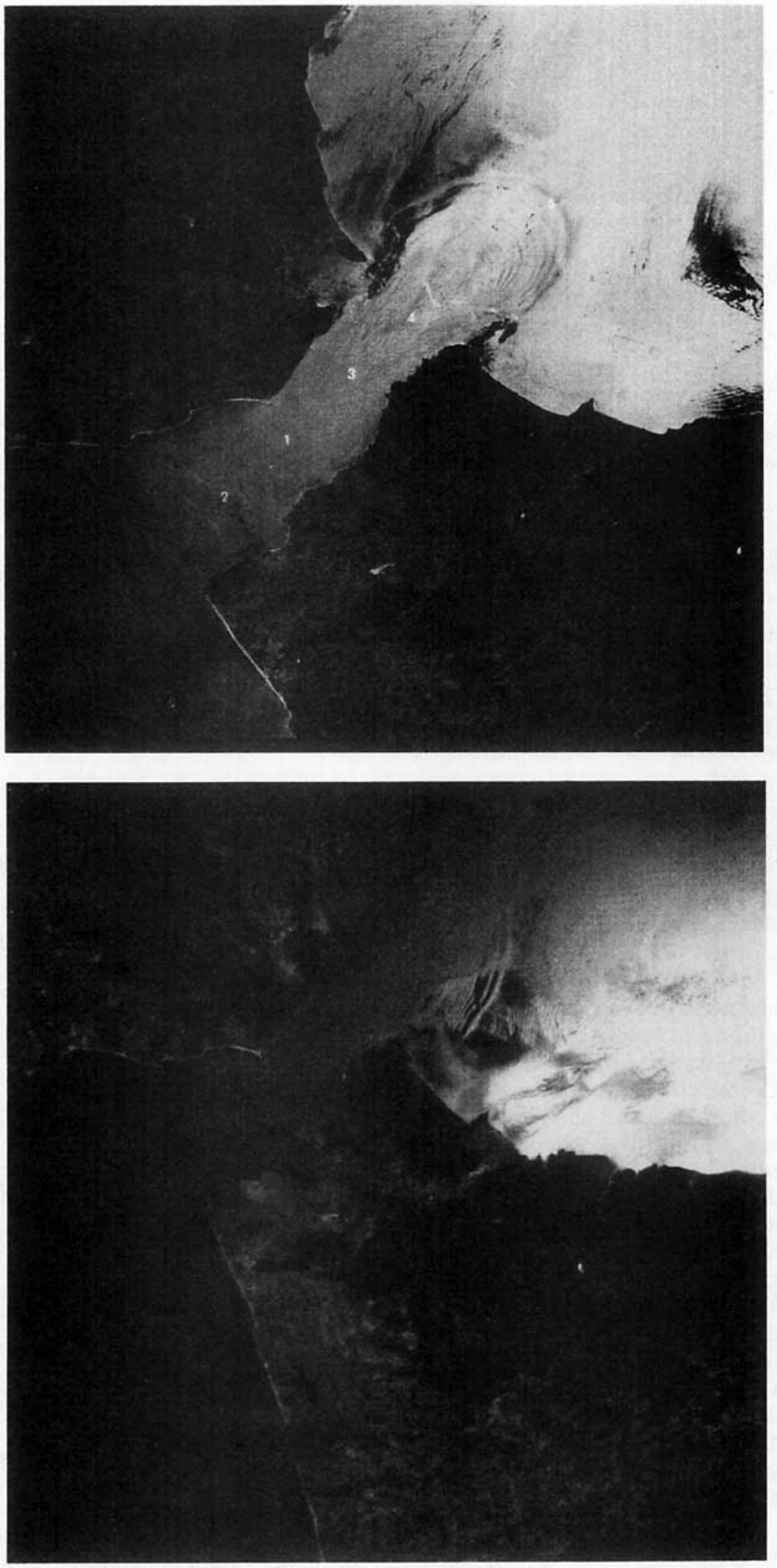

FIG. 1. Photographs of the Strait of Gibraltar taken from the Space Shuttle *Challenger* in October 1984. They show trains of internal solitary waves propagating into the Alboran Sea (National Aeronautics and Space Administration).

where the effect of advection of the wave due to the presence of a strong Atlantic Water jet flowing into the Alboran Sea is also considered. It is important to note that such an initial wave that cannot be compared with any data—the generating parameters relative to Kinder's measurements being unknown—is in agreement with typical values of an interface depression derived from the initial eastward propagation of the semidiurnal tide generated just west of the Camarinal sill. The problem of the generation of internal tides over sills and their evolution in a channel is therefore very important in this context and will be discussed in section 3.

Two more points will be addressed: namely, the reason why sometimes solitary wavetrains are detected in the Alboran Sea while other times borelike waves are recorded, and the observed connection between the appearance of packets of strong internal solitary waves and the weakening of the anticyclonic Alboran Sea gyre. Theoretical analyses providing answers to these two problems will be presented in sections 5 and 6. In the next section we will start by describing the model equation used in our numerical experiments.

2. A model for the propagation of 2-D nonlinear long internal waves

The one-dimensional and unidirectional propagation of weakly nonlinear, long (with respect to a typical vertical length scale related to stratification) internal gravity waves is described by different evolution equations depending on whether the wavelength is much smaller, comparable to or much larger than the total water depth H. In the first case the evolution is given by the Benjamin-Ono equation (Benjamin 1967; Ono 1975), in the second case by an equation proposed by Joseph (1977) and Kubota et al. (1978) and, finally, for shallow-water waves by the Korteweg-de Vries equation:

$$\eta_t + c_0\eta_x + \alpha\eta_{xxx} + \beta\eta\eta_x = 0 \qquad (1)$$

where η is the pycnocline displacement (the coefficients c_0, α and β will be specified later), originally derived for long surface gravity waves. For the internal solitary waves observed in the Alboran Sea a typical horizontal length scale is $L = O(2\text{ km})$ and in the region of propagation under consideration the average water depth is $H \approx 1200$ m, thus we are in a range for which both second and third evolution equations could apply. However, although the second equation might appear more appropriate, validity of the KdV equation has been shown even for waves whose length is only slightly greater than the total depth (Koop and Butler 1981; Segur and Hammack 1982). Note also that Osborne and Burch (1980) used the KdV equation to derive quantitative information in agreement with experimental observations for the internal solitons in the Andaman Sea, for which $L/H \approx 2$, as in our case. We will therefore make use of the KdV dynamics in its weakly two-dimensional version (see below).

The KdV equation was first derived for internal waves by Benjamin (1966), but its validity for surface waves was known well before (Korteweg and de Vries 1895). The validity of KdV for both long surface and internal waves is a consequence of (i) the same phase dispersion of such wave systems in the limit $L \gg H$ (represented by the term $\alpha\eta_{xxx}$), namely

$$\omega \approx c_0 k - \alpha k^3,$$

where ω is the angular frequency, k the wavenumber and c_0 the phase speed of infinitely long (nondispersive) waves, and of (ii) the same kind of steepening effects represented by the term $\beta\eta\eta_x$ in (1) implying that the correction to c_0 for the speed of a point on the wave due to finite amplitude effects is simply proportional to the amplitude at that point [for example, see Dodd et al. 1982, for an extensive discussion of the mathematical properties and physical applications of (1)].

In the Alboran Sea one has a fairly thin pycnocline separating two distinct water types, the North Atlantic central water and the deep water of the western Mediterranean (Lacombe and Richez 1982); moreover the waves we want to model have a clear first-mode vertical structure (Kinder 1984). This justifies the use of a two-layer fluid model as a good first approximation. Note that a two-layer system was also used by Preller (1986), to study the Alboran Sea gyre. With the definition of Fig. 2 the coefficients in (1) for a two-layer system read (e.g., Segur and Hammack 1982):

$$c_0 = \left[g'\frac{H_1H_2}{H}\right]^{1/2}, \quad \alpha = \frac{c_0}{6}H_1H_2,$$

$$\beta = \frac{3}{2}c_0\frac{(H_1 - H_2)}{H_1H_2}, \qquad (2)$$

where $H = H_1 + H_2$ and $g' = g\Delta\rho/\rho$ is the reduced gravity. Note that unlike in the case of surface waves, here the sign of β can be both positive and negative. This implies that, while for surface waves solitons represent a positive displacement of the free surface, for

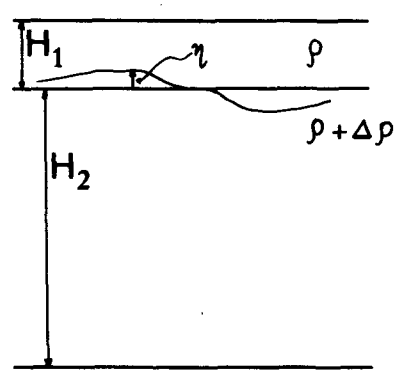

FIG. 2. The two-layer ocean model used in the present analysis.

internal waves they can be either positive or negative. In the present case they will be solitary waves of depression because $H_1 < H_2$.

Equation (1) was used by several authors to model long internal solitary waves (see section 1). In all cases the 1-D assumption was acceptable—thanks to the geometry of the basins and generation regions involved. On the other hand, for the internal solitons in the Sulu Sea (Liu, A. K. et al. 1985), a generalized Kubota equation (Kubota et al. 1978) was used in which 2-D effects were taken into account through a parameterization of the radial spreading of the wave. For the waves observed in the Alboran Sea it is clear from Fig. 1 that the 1-D approximation cannot be introduced either. Use will therefore be made of the Kadomtsev–Petviashvili (1970) equation

$$\frac{\partial}{\partial x}\left[\eta_t + c_0\eta_x + \alpha\eta_{xxx} + \beta\eta\eta_x\right] + \frac{c_0}{2}\eta_{yy} = 0, \quad (3)$$

that represents the 2-D generalization of (1) for 2-D waves predominantly traveling along x and whose spatial variation along y is small compared with that along x: $(Ly/Lx)^2 \gg 1$. In this sense (3) applies to "weakly" 2-D waves. Equation (3), in a more general form for continuously stratified fluids and with rotation, was derived by Grimshaw (1985) and used by Katsis and Akylas (1987) to study the effect of rotation on internal solitons in a channel. David et al. (1987) have recently extended (3) (for surface waves) to take into account weak variations in water depth and width of the channel.

Here we shall adopt a slightly different version of (3) (Pierini 1986):

$$\frac{\partial}{\partial x}\left[\eta_t + c_0\eta_x - \frac{\alpha}{c_0}\eta_{xxt} + \beta\eta\eta_x\right] + \frac{c_0}{2}\eta_{yy} = 0, \quad (4)$$

which is the natural 2-D generalization of the so-called PBBM (Peregrine 1966; Benjamin et al. 1972) or "regularized long wave" (RLW) equation. Equation (4) is basically equivalent to (3) and can be derived from it by substituting one x-derivative in the dispersive term with a time derivative according to

$$\eta_t + c_0\eta_x = 0,$$

i.e., equation (1) at lowest order (dispersive and nonlinear effects are small and act on a time scale much larger than L/c_0). A numerical scheme for PBBM or (4) has the advantage of allowing for the presence of spurious short waves in the initial condition without the growth of numerical instabilities, thanks to the peculiar dispersion relation for large wavenumbers (see Benjamin et al. 1972, for a discussion of this point). It is to be noted that while the initial-value problem for the KdV or KP equations is exactly solvable by means of the inverse-scattering method, the same problem for the PBBM or (4) equations is not. Nonetheless the solution of PBBM has been shown to exhibit true soliton behavior (Eilbeck and McGuire 1977). Moreover the solutions of KdV and PBBM for the same initial condition are found to be very close together, even for large amplitudes (Bona and Smith 1975; Eilbeck and McGuire 1977). No results of this nature are available for the weakly 2-D case, but the solutions of (3) and (4) are certainly expected to be close together in the same sense as for the 1-D case.

In the present study Eq. (4) will be solved numerically using the implicit, leapfrog finite difference scheme by Pierini (1986). Hence, when reference is made of the KP equation, its regularized version (4) is understood. Note also that the term "soliton" will be used in a broad sense. First of all in the 1-D limit our solitons will be solutions of the PBBM equation rather than the KdV equation, although the difference between the two is thoroughly negligible in the present context. Moreover, we will sometimes call "solitons" also the 2-D solitary waves described in sections 4–6 that have not been shown to exhibit a real soliton behavior.

3. The generating mechanism and the initial stage of propagation

Trains of internal waves resulting from evolution of the internal semidiurnal tide generated in the Strait of Gibraltar were first detected in the early 1960s by different investigators (e.g., Frassetto 1964; see Boyce 1975 for a review). The measurements involved were all performed within the strait both west and east of the main sill and important asymmetries were found due to the asymmetry in the bottom topography and geometry of the strait. More recently Kinder (1984) described a 110-day-long series of current measurements taken about 45 km east of the strait during the international oceanographic expedition "Donde Va" and reported the arrival of packets of internal solitary waves at intervals of 12–13 hours. Kinder's findings confirm in a definitive way that internal solitary wavetrains traveling eastward into the Alboran Sea can be observed, resulting from the evolution of a longer, compact internal tidal wave generated from the interaction of the M_2 tidal current with the sill in the strait (see the next section for details).

Let us now consider separately (i) the generation of internal waves through the interaction of a flow with topography and (ii) the initial stage of propagation within the strait. In the next section we will therefore be ready to consider a realistic waveform inside the strait whose evolution in the Alboran Sea can explain the measurements described by Kinder.

a. Generation of internal tides over a sill

Long (1954) has studied experimentally and analytically the stationary deformation of the interface separating two fluids, derived from the interaction of a barotropic flow with an underwater barrier. In the case

of the present study in which the lower layer is deeper than the upper, basically three different regimes can be identified. For sufficiently small Froude numbers $Fr = U/\sqrt{g'H}$ (where U and H are the upstream values of the mean flow and water depth) an "absolutely subcritical" regime exists for which a slight depression of the interface over the barrier or a small downstream lee wave (for sufficiently small obstacles) is produced. For moderately supercritical values of Fr[$Fr \geq Fr_c$, where Fr_c depends on the values of the parameters involved (see section 6)] a higher amplitude disturbance is observed, namely, a hydraulic jump of depression at the lee while for larger supercritical values (and for large obstacles) the interface rises upstream, reaches a maximum value over the crest of the barrier and experiences a sudden drop on the lee. This third waveform is denoted as "hydraulic drop" by Long.

The main limitation of Long's study, as far as our problem is concerned, lies in the assumption of stationary flow, but assuming that the hydraulic adjustment is fast enough, useful information can be obtained for the stage of formation of the disturbance. However, since such a disturbance is virtually steady while superimposed on the mean flow U, when the tide slackens the wave must travel upstream, thus maintaining its speed with respect to the surrounding fluid. When the tide reverses the wave increases its speed (in the frame at rest) being advected by the tide itself and finally leaves the sill. This is the basic mechanism for internal tide generation in the Strait of Gibraltar. A similar qualitative behavior was observed in laboratory experiments by Maxworthy (1979), through acoustic images by Farmer and Smith (1980) in the Knight Inlet and by Haury et al. (1979) in Massachusetts Bay. Recently, Hibiya (1986) proposed a linear analytical model for the generation of internal waves in continuously stratified fluids by tidal flow over a sill. The time evolution during the generating stage leads to either a fairly symmetrical oscillation or to an asymmetric wave similar to a hydraulic drop, for weak or strong tidal flow respectively. The linearization of the dynamics, though necessary in an analytical treatment, is, however, rather restrictive in this context.

We conclude this subsection by comparing qualitatively these theoretical results with in situ observations. Figure 3 taken from the paper by Lacombe and Richez (1982) gives the internal waves of salinity during two tidal cycles at the sill. Note that if the sill were symmetrical one would expect two highs and two lows in one tidal period at a fixed point at the sill because of the superposition of a right running and a left running wave with a 180° lag. The appearance of just one main high and one main low can be explained on the basis of the asymmetry of the strait geometry and topography. Indeed, as Boyce (1975) points out, there is evidence of strong propagating internal fronts only on the eastern side of the strait. Therefore the oscillation of the interface evident in Fig. 3 is to be accounted for by an eastward propagating tidal wave. Following the terminology used by Hibiya (1986) it appears to be a wave of intermediate strength between the weak and moderate flow regime. The generation will be analyzed further on in section 6 where the possibility of passing from one regime to another as a consequence of the variability of the mean Atlantic water inflow will be discussed.

b. The initial stage of propagation

Before analyzing the initial evolution of a wave traveling eastward inside the strait, let us briefly review the possible types of behavior allowed, in general, by Eq. (1). Let us consider the Ursell number defined as the ratio between nonlinear and dispersive terms in (1), i.e., $Ur = AL^2/h^3$, where A is a typical amplitude, L is a characteristic length scale and h is the water depth for surface waves or

$$h = [(H_1^2 H_2^2)/|H_1 - H_2|]^{1/3}$$

for internal waves in a two-layer system, obtained by evaluating O(Ur) through the ratio

$$(\beta A^2/L)/(\alpha A/L^3)$$

with α and β given by (2). If the initial Ursell number is $Ur_0 \gg 1$ then nonlinear effects are initially predominant, the wavefront tends to steepen, L decreases together with Ur until $Ur \sim 1$ by which time a train of n solitons is formed where, roughly, $n = O(Ur_0)$ for large n. If, on the other hand, $Ur_0 \ll 1$ dispersive effects are initially predominant, the wavefront tends to the Airy phase, its amplitude decreases as $t^{-1/3}$ (in the 1-D case) but L increases as $t^{1/3}$ in such a manner that Ur grows with time as $t^{1/3}$ until, again, $Ur \sim 1$, by which time one soliton is formed followed by a dispersive tail. Note that in the first case the solitonic state [for which Ur = O(1)] is reached after a much shorter time.

In the eastern side of the Strait of Gibraltar one has roughly $H_1 \approx 150$ m, $H_2 \approx 350$ m, so $h \approx 240$ m, moreover for the initial wave of Fig. 3, $A \approx 50$ m and $L \approx 5000$ m (≈ 1 h $\times$ 1.4 m s^{-1}), therefore, $Ur_0 \approx 90$ and consequently the wave should experience strong steepening effects. Unfortunately there are no data available on its evolution but a waveform at a location farther east is available (Fig. 4). It was taken only about two days before that of Fig. 3 so its form at the sill was probably not very different from the latter. The steepening effects are strikingly evident, as expected.

4. A solitary wavetrain detected in the Alboran Sea: Comparison between experimental and theoretical values

Let us start by describing briefly the measurements reported by Kinder (1984). Long time series of current data were taken during the period June–October 1982 at ~45 km east of Gibraltar in five different positions by means of acoustic current meter moorings (Fig. 5).

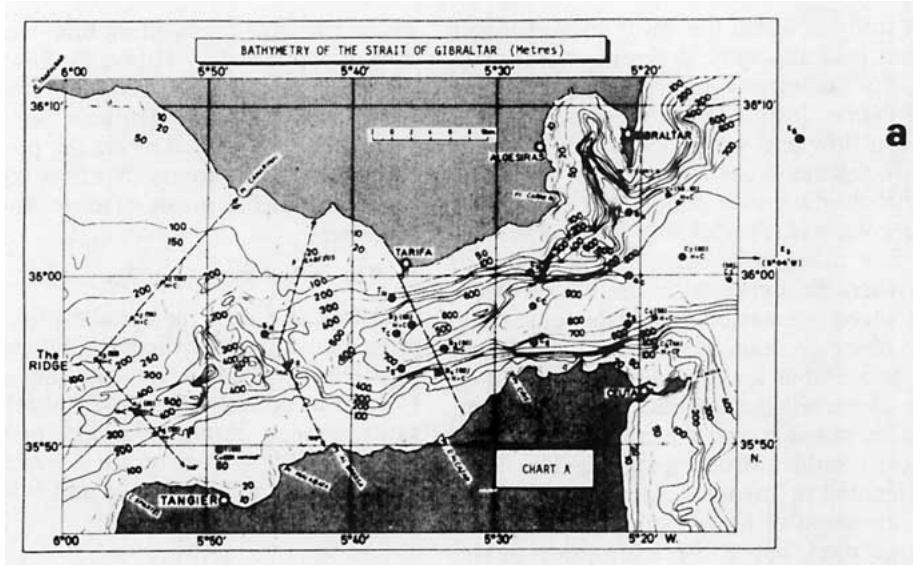

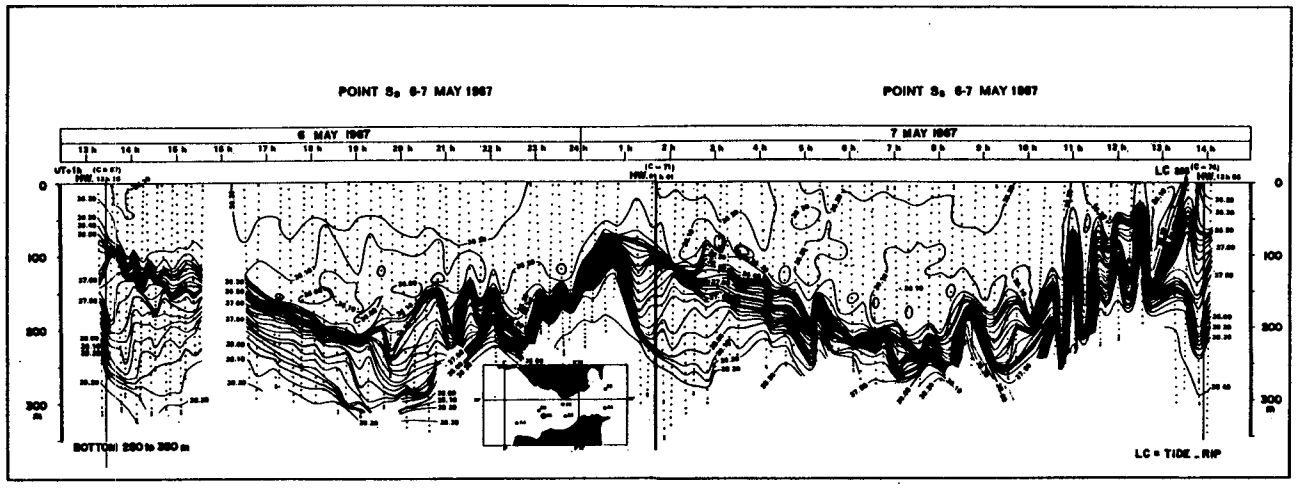

FIG. 3. (a) Bathymetry of the Strait of Gibraltar and (b) example of an internal wave of salinity during two semidiurnal tidal cycles near the sill (after Lacombe and Richez 1982).

Data were taken above and below the pycnocline so that first-mode internal waves could be resolved. At each instrument packets of waves were recorded more than once per lunar day throughout the whole period of measurements, the interval between the arrival of two successive packets being 12–13 hours (the semidiurnal period). Such wave packets were, sometimes, borelike, some other times they were composed of a train of solitary waves (the most energetic events). In the paper quoted above the data of the strongest wavetrain were presented (Fig. 6): they show a train of internal solitons in which the ratio between the velocities in the upper and in the lower layer is in good agreement with the theoretical value for small amplitude internal waves in a two-layer ocean. The data relative to mooring 15 have been kindly provided to the author by T. H. Kinder (see Fig. 11). Note, however, that no information is available on the internal tide generated inside the Strait of Gibraltar whose evolution led to this wavetrain.

Now, the main aim of this paper is:

(i) to present an initial wave in the strait that, evolving according to (4), develops into a set of internal waves that are in good agreement with Kinder's data in points close to positions 12 and 15. Moreover such an initial wave (that cannot be compared with any data, as already mentioned) must at least be acceptable as an internal tide in the Strait of Gibraltar as far as its amplitude, length and shape are concerned, according to the discussion of the preceding section.

(ii) to explain why and under which circumstances an internal tide develops into a train of solitons or into a more or less steep, compact wave.

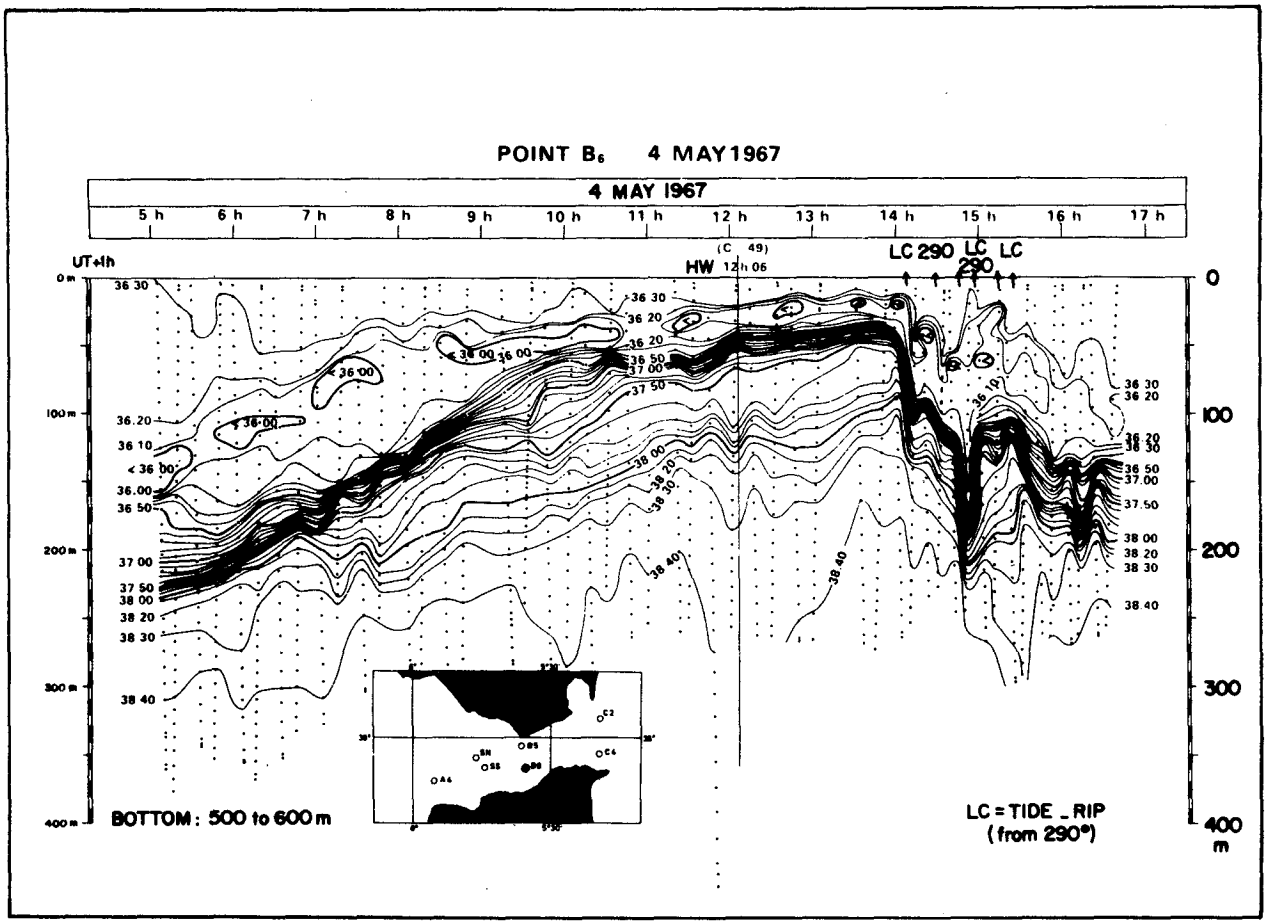

FIG. 4. Example of an internal wave of salinity in the south of Tarifa section, at about 15 km east of the sill (after Lacombe and Richez 1982).

Point (i) will be considered below, while point (ii) will be analyzed in the next section.

We have solved Eq. (4) in a domain as in Fig. 5. The free-slip boundary conditions

$$\eta_y = 0$$

have been imposed along the rigid boundaries while the interface displacement has been prescribed as a function of time along the line AB. The following typical values of the various parameters have been chosen: $\Delta\rho/\rho = 0.002$, $H = 1200$ m ($H_1 = 200$ m, $H_2 = 1000$ m). The dimensions of the domain are AB = 13 km, ZO = 30 km, CD = 112.6 km. It should be stressed that the solid boundaries at $y = \pm 56.3$ km are never "touched" by the wave in the numerical experiments we are going to discuss, so that the wave travels into a semi-infinite ocean, as in fact occurs. The grid and time steps are $\Delta x = 100$ m, $\Delta y = 2166$ m, $\Delta t = 55.3$ s [with this choice of Δt the nondimensional time step $\Delta t' = (g'/H)^{1/2}\Delta t = 0.22$ equals the nondimensional grid step $\Delta x' = (H_1 H_2)^{-1/2}\Delta x$ so that $c_0' = 1$, which is somewhat advantageous in handling the numerical scheme].

The interface depression along AB is chosen as (Fig. 7):

$$\eta(t) = \begin{cases} A \exp\left[-\left(\dfrac{t - t_0}{T_1}\right)^2\right], & t < t_0 \\ A \exp\left[-\left(\dfrac{t - t_0}{T_2}\right)^4\right], & t \geq t_0 \end{cases} \tag{5}$$

where $A = -75$ m, $T_1 = 0.4$ h, $T_2 = 5$ h and $t_0 = 1$ h. We assume a very steep wavefront [see section 3b] whose slope is comparable with observed values for a wave taken at about the same location in the strait (e.g., see Fig. 4 between 14–15 h). This first part of the internal tide (for $t < t_0$) determines, among other things, the time after which the solitary wavetrain develops (see the next section). On the other hand, the second part (for $t \geq t_0$) contributes to determine the total energy of the wave, the number of solitons and some of their characteristics. The amplitude of the depression is also comparable with those measured. Note, however, that the actual depth along AB is only about 65% of H and

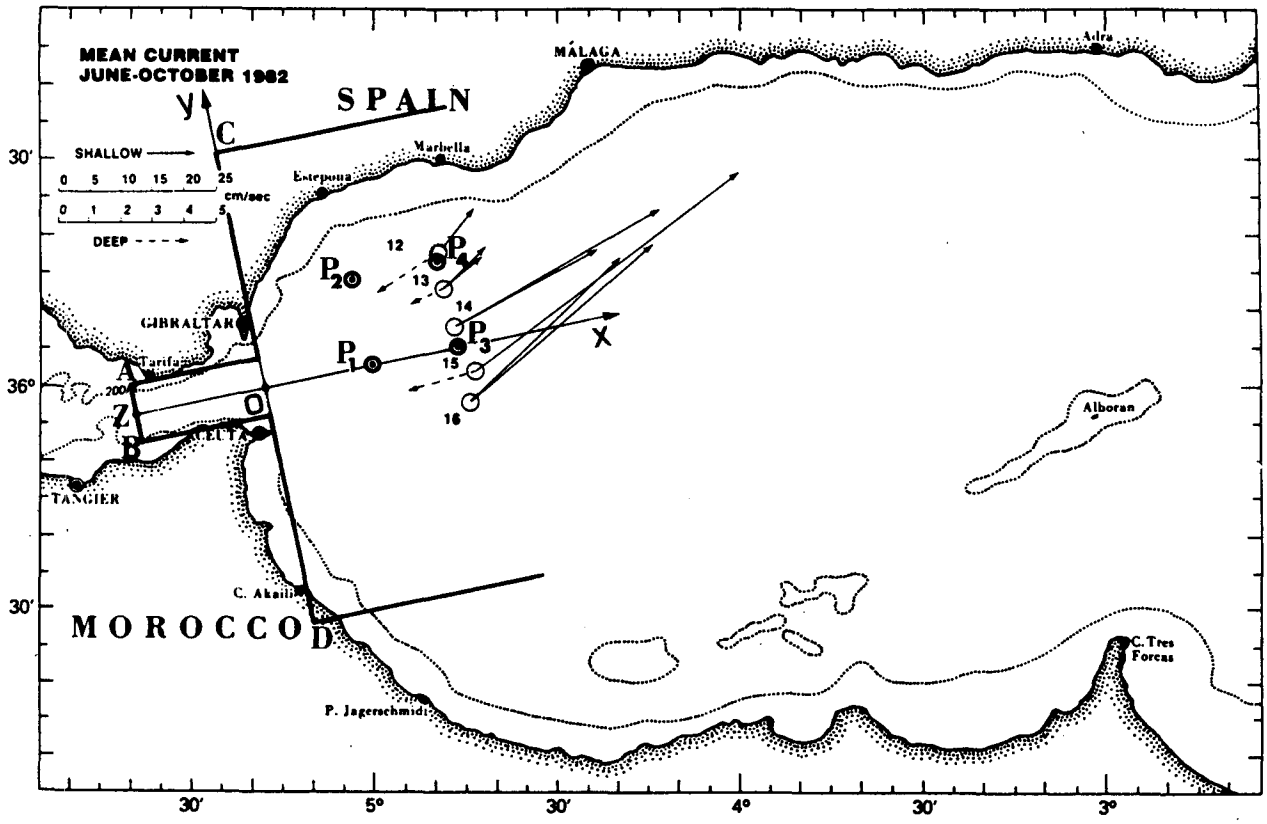

FIG. 5. Positions of current meter moorings 12–16 where current measurements were taken during the "Donde va" oceanographic experiment, with the corresponding 110-day-record means (Kinder 1984). The domain of integration of Eq. (4) is also shown. All the heavy lines are rigid boundaries except for the line AB along which the interface depression is prescribed as a function of time. Numerical time series have been taken in points $P_1 = (25, 0)$, $P_2 = (25, 19.5)$, $P_3 = (45, 0)$ and $P_4 = (45, 19.5)$ (in km).

that the slow variation of bottom topography within the strait has been neglected. Therefore, these values of A, T_1 and T_2 are slightly different to those appropriate for a model that was to include topographic effects.

Moreover, let us stress that although the wave travels (predominantly) along x in channels of constant width

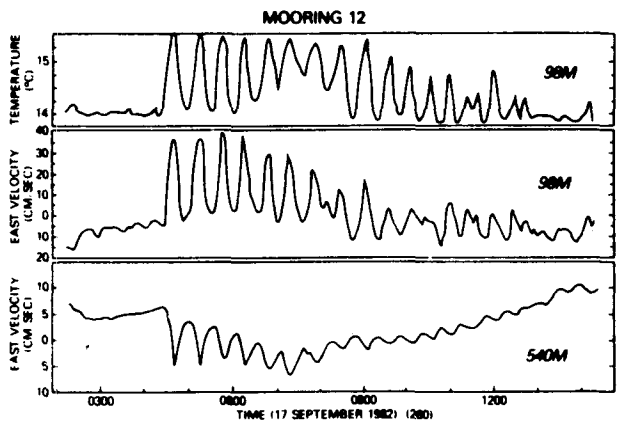

FIG. 6. The most energetic packet of internal solitary waves of the 110-day record as measured at mooring 12 (after Kinder 1982).

both for $x < 0$ (in the strait) and for $x \geq 0$ (in the Alboran Sea), so that no additional term must be added to the equation of motion (4) (for a channel of slowly varying width such term has been calculated by David et al. 1987 for surface waves), some undesirable effect could nonetheless be expected around $x = 0$ where the width increases sharply. However Δy has been chosen in such a way to be about as large as a typical length scale of the wave along x, so that the assumption of weakly 2-D waves required for the KP equation is met reasonably well also for $x \approx 0$. As a result of this, a very smooth transition of the wave through the mouth of the strait has been observed in all of the numerical experiments. Another problem that might arise in connection with a variation of channel width is that discussed by Miles (1979) for the KdV equation in slowly varying channels. The implicit neglect of the weak reflection that accompanies the gradual variation of the channel for that model leads to the nonconservation of mass. A similar problem could be expected for the KP equation in a similar situation. Here, however, the very fact that the variation is not weak leads to a diffracted wave that does not feel the lateral boundaries while propagating into the Alboran Sea, which is initially a semi-infinite ocean in our model; therefore no

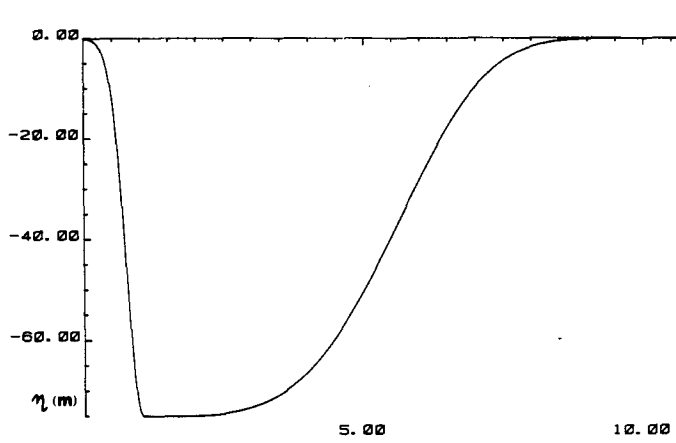

FIG. 7. Initial wave used in the numerical experiments of section 4 and given by formula (5).

significant variation in mass should be found. This has been checked numerically and, indeed, the mass of the diffracted wavetrain has been found to correspond to that of the initial internal tide inside the strait within 2%. When the wavetrain has eventually reached the lateral boundaries of the Alboran Sea a variation in mass is found near the boundaries themselves, in agreement with Miles's (1979) analysis. However this does not affect the present numerical results because they refer to times for which the wave is still traveling in a semi-infinite ocean.

It is also to be noted that the Coriolis force has been neglected altogether. This is quite acceptable for the evolution in the Alboran Sea because the waves are highly superinertial and do not interact with the lateral boundaries. Within the strait, however, the situation is different because the wave extends all across it and a fast semigeostrophic adjustment is to be expected with a consequent formation of an internal Kelvin wave (Pratt 1983; Renouard et al. 1987), whose associated cross-channel variation has in fact been observed in field data (Lacombe and Richez 1982). However, numerical experiments show that the cross-channel variations that would be present at the mouth of the strait are quickly lost during propagation into the open sea. Thus, as we are mainly interested in the wave field in this second portion of the domain, the assumption $f = 0$ appears reasonable. Eddy viscosity and bottom friction are also neglected in the equation of motion under the assumption that such effects are not important over a time scale such as that of the present study. Finally we note that in order to eliminate numerical instabilities similar to those described in Pierini (1986), we have cut them out of the strait—where they develop near the line AB—by shortening the channel (i.e., by redefining it from -30 km $< x < 0$ to -12 km $< x < 0$) after the wave has completely left it.

We are now ready to discuss the results of the numerical experiments in connection with the experimental data. Figure 8 shows the 3-D display of the state of the interface at two different times, $t_1 = 9.22$ h and $t_2 = 12.3$ h, while Fig. 9 gives the wave profiles for $y = 0$ and $y = 19.5$ km at $t = t_1$ and $t = t_2$. Figure 10 gives the current time series in the upper layer $U_1(t)$ at points $P_{1/2/3/4}$ of Fig. 5 computed from the interface displacement by means of the relations:

$$U_1 = -\frac{c_0}{H_1}\eta, \quad U_2 = \frac{c_0}{H_2}\eta,$$

where U_1 and U_2 are the upper and lower layer velocities, respectively. These formulae can be easily obtained by assuming as a first approximation

$$\begin{cases} U_{1t} \approx -g\eta'_x \\ U_{2t} \approx -g\eta'_x - g'\eta_x \\ \dfrac{\partial}{\partial x} \approx -\dfrac{1}{c_0}\dfrac{\partial}{\partial t} \end{cases}$$

where η' is the sea surface displacement, and taking into account the relation between η' and η given by

$$\eta' = -\left(\frac{\Delta\rho}{\rho} H_2/H\right)\eta.$$

The time series 10c, d relative to P_3 and P_4 have been compared with Kinder's data reported in Fig. 11. The results are shown in Table 1 in which the soliton length has been arbitrarily evaluated at ⅓ of the crest-to-trough amplitude, where the shape of the soliton is well defined both in numerical and experimental data. The amplitude of the first soliton in P_3 is in very good agreement with the corresponding experimental value; this is not surprising because the parameters in (5)—in particular T_1—have been calibrated in such a way as to achieve this result. On the other hand, the fact that the agreement is good also in P_4 implies that the (nonlinear) spreading of the wave is modeled fairly ac-

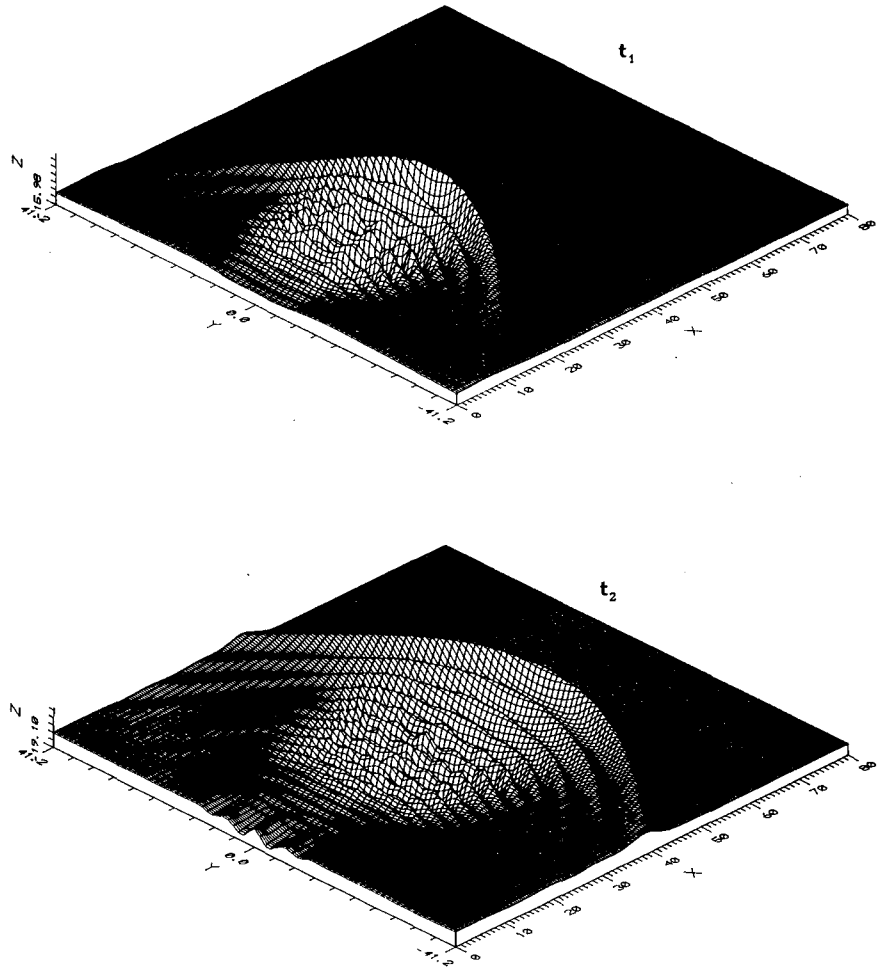

FIG. 8. Numerical internal waves (-100η) at times $t_1 = 9.22$ h and $t_2 = 12.3$ h. Note that the resolution along y is half that shown in the figure, for which a spline routine has been used; the actual resolution along x is 5 time larger. Note also that the lateral boundaries in the figure do not correspond to the rigid boundaries at $y = \pm 56.3$ km (x and y are in km and z in m; the values $z = -15.98$ and -19.10 are the z-coordinates of the basis of the 3-D figures).

curately by the KP equation in this context (note that the degree of agreement in P_4 is too high to be totally significant and should—to some extent—be considered as casual). The length of the first soliton is also in good agreement at both points although the relative error is slightly greater.

The subsequent solitons have been reproduced by calibrating the parameter T_2 in (5). The agreement between numerical and experimental data as far as the second solitary wave is concerned is not as good as for the first one, but it is nonetheless sufficiently good. In this regard let us emphasize that if one considers the relative simplicity of the mathematical model, a much better agreement could neither be expected nor be considered meaningful. It is rather to be stressed that despite the simplicity of such an approach all but one of the main features of the internal wavetrain in Fig. 11 can be theoretically reproduced within an acceptable quantitative agreement.

There is one important discrepancy that we are now going to discuss. Consider the difference $\Delta\tau$ between the time at which the first solitary wave reaches P_3 and that at which it reaches P_4. The experimental and theoretical values are

$$\Delta\tau_{\text{observed}} \approx 1.5 \text{ h}, \quad \Delta\tau_{\text{theoretical}} \approx 0.7 \text{ h}.$$

This difference is clearly to be accounted for by the advection of the wave due to the presence of a strong sheared current in a "beam" approximately aligned with the strait, namely the Atlantic water jet superimposed on the deeper and weaker Mediterranean water outflow—an effect not included in the model. This is also confirmed by the images of Fig. 1 where the higher curvature of the wavefronts in the central part of the wavetrain is evident.

A rough calculation can help to understand the observed discrepancy. Let us consider the Doppler-shifted

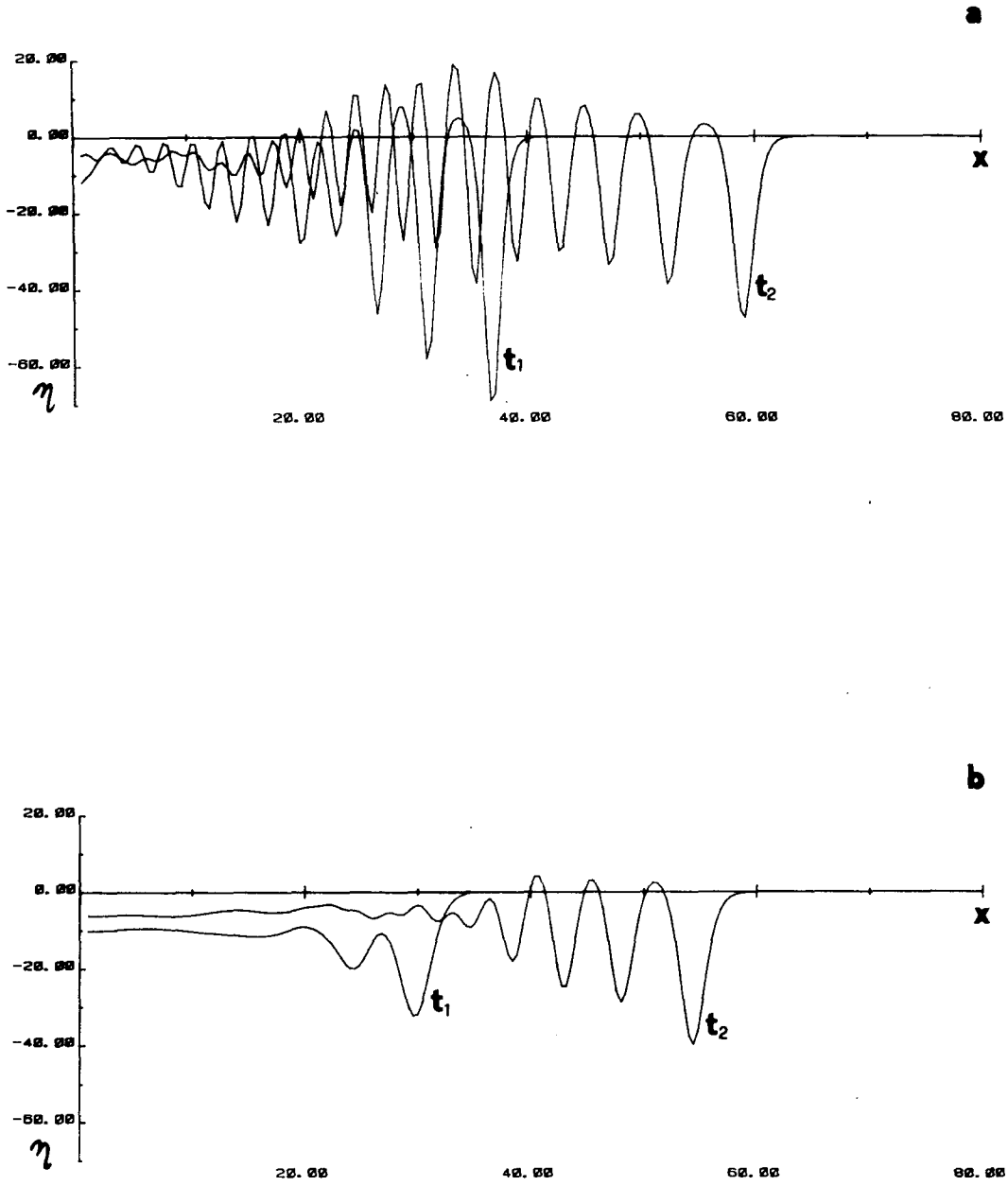

FIG. 9. Wave profiles at t_1 and t_2 along the segment $0 < x < 80$ km for $y = 0$ (a) and $y = 19.5$ km (b) (η is in m).

phase speed of a long internal wave in a two-layer ocean in the presence of a sheared current,

$$\bar{c}_0 = \frac{H_1 U_2 + H_2 U_1}{H} + \left[g' \frac{H_1 H_2}{H} - \frac{H_1 H_2}{H^2} (U_1 - U_2)^2 \right]^{1/2}, \quad (6)$$

and suppose that around $y = 0$ the wave is advected with speed $\bar{c}_0$ given by (6) while it is advected with speed c_0 along $y = 19.5$ km (Preller 1986 has shown that the Atlantic jet is weakly divergent so that in the region under consideration the current is virtually confined in the beam $-AB/2 < y < AB/2$). Let us also assume that, as a first approximation, the wave is adiabatically advected by this nonhomogeneous current field, in such a way that the waveforms of Fig. 10c, d would still be measured in points P_3 and P_4. Taking the typical values $U_1 = 40$ cm s^{-1} and $U_2 = -8$ cm s^{-1} (corresponding to a zero net flux through the strait) $\Delta\tau_t$ would increase to

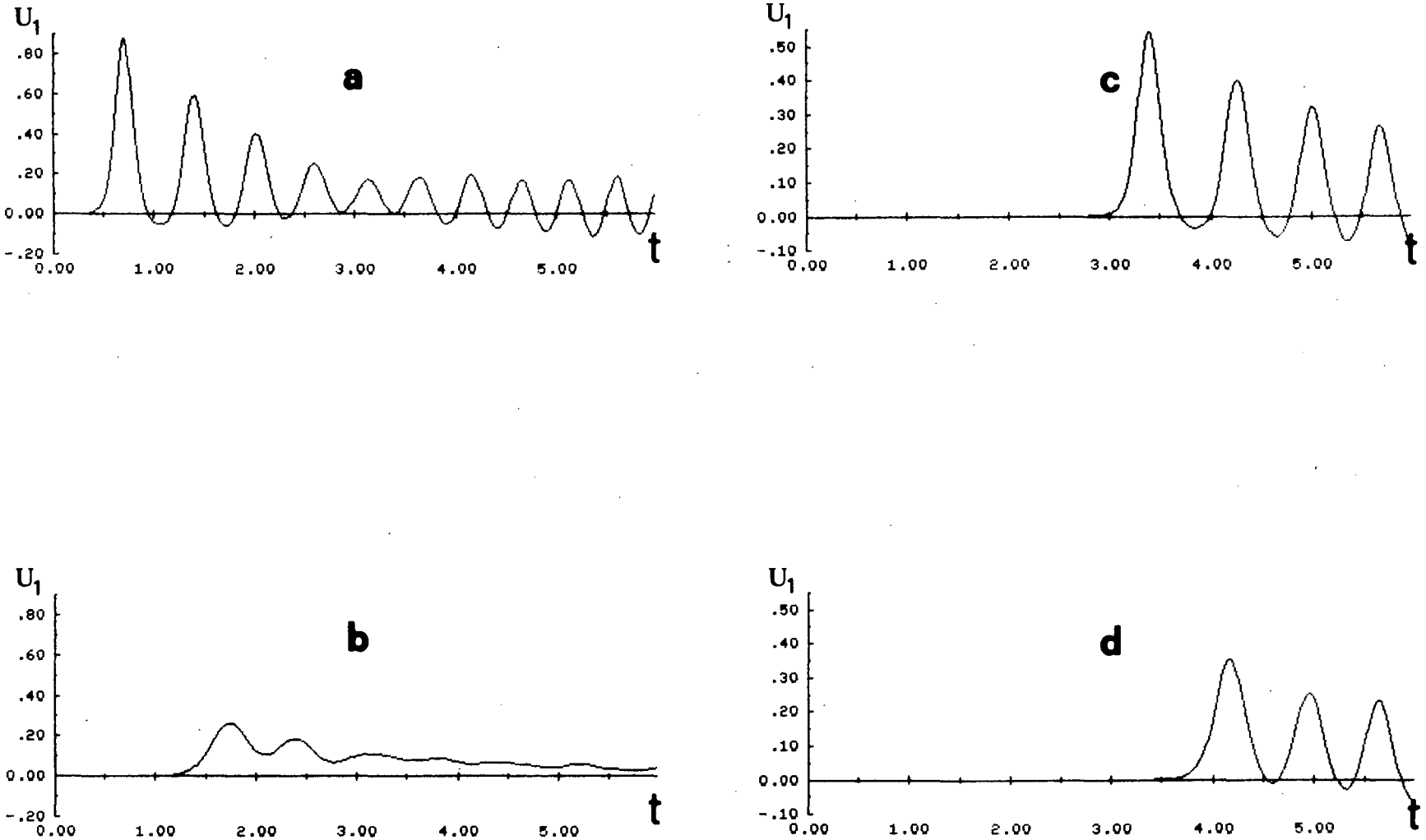

FIG. 10. Numerical current time series at points $P_{1,2,3,4}$ (*a*, *b*, *c*, *d*, respectively). The time origin in the figures corresponds to $t = 6.93$ h (U_1 is in cm s^{-1} and t in h).

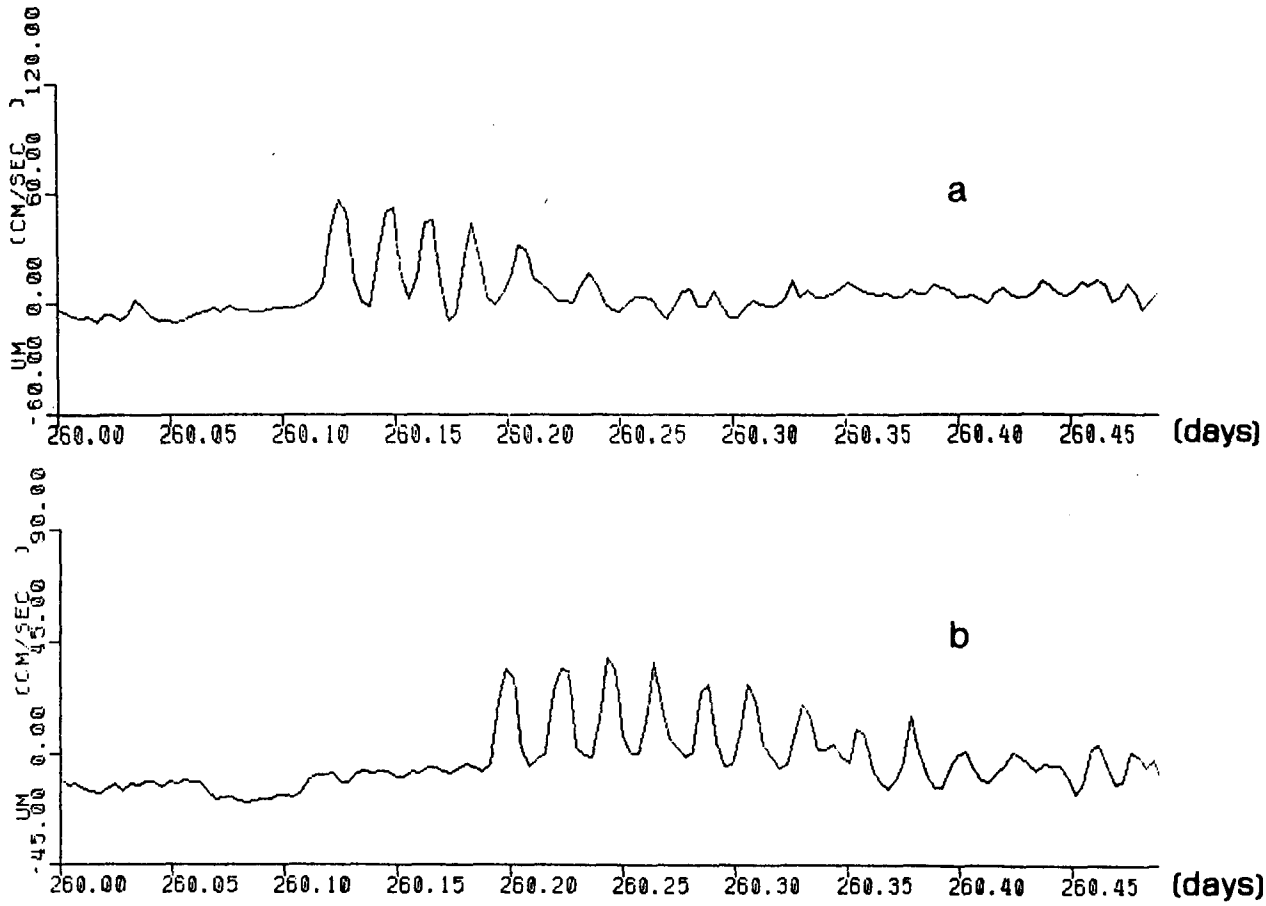

FIG. 11. Time series of the eastward component of the current in the upper layer measured at moorings 15 (a) and 12 (b). Figure 11b coincides with Fig. 6 while Fig. 11a represents unpublished data (courtesy of T. H. Kinder).

$$\Delta\tau_{\text{theoretical}} \approx 1.3 \text{ h},$$

in better agreement with the observed value. Obviously the nonlinear internal wavefield interacts with a vertically sheared current in a much more complex way (e.g., Tung et al. 1981), but for small periods of time advection is, in fact, the predominant effect.

TABLE 1. Comparison between experimental values relative to moorings 15 and 12 and theoretical values relative to points P_3 and P_4, respectively. The subscripts 1 and 2 refer to the first and second soliton, respectively. The soliton length is evaluated at ⅓ of the crest-to-trough total amplitude.

	Experimental values (±10%)	Numerical values (±5%)
	P_3	
U_1 (cm s^{-1})	55	54
U_2 (cm s^{-1})	51	44
L_1 (h)	0.30	0.32
L_2 (h)	0.27	0.35
	P_4	
U_1 (cm s^{-1})	34	35
U_2 (cm s^{-1})	32	27
L_1 (h)	0.26	0.41
L_2 (h)	0.27	0.38

5. Sensitivity of the evolved wave to changes in the initial wave at the generation site

During the 110-day-long current meter records analyzed by Kinder (1984) solitary wavetrains were not always observed: "sometimes waves were totally absent, and sometimes the packets were bore-like with small individual waves superimposed on them." In other words the amplitude and form of the internal semidiurnal tide generated west of the major sill (section 3a) undergoes important variations—over a time scale of several days—in such a way that the evolved wave may or may not be composed of solitary waves at a distance 45 km east of the strait. These variations are related to the spring tidal cycle and to variability of the mean flow in the strait and such a relation will be considered in the next section. In this section we will restrict ourselves to studying the character of the evolution of an initial wave prescribed along the line AB for different values of A, T_1 and T_2 disregarding the physical mechanism that determines these values. This amounts to

analyzing the sensitivity of the model results to changes in the initial conditions.

Let us start by considering an idealized situation in which the wave travels in a rectangular channel with rigid lateral boundaries at $y = \pm AB/2$ (no Alboran Sea, longer Strait of Gibraltar!; the real case will be considered later). In such a case the Korteweg-de Vries equation applies. Let us also restrict ourselves to initial waves with initial Ursell numbes Ur_0 much larger than unity, as appropriate for the case under consideration (see section 3b). For them the initial evolution will be characterized by the steepening of the wavefront due to nonlinearities, the dispersive effects being negligible.

Now we would like to answer the question: after how long (and therefore at what distance from AB) is the first soliton expected to begin to form? A very simple calculation can provide the answer. Let us define $L_0 = T_1 c_0$ as the initial length scale of the wave at its leading edge: such a length will decrease in time because of the steepening of the front, until it reaches the value L_s for a soliton whose amplitude is approximately given by the initial amplitude A_0 (note that during the initial propagation the maximum amplitude does not change appreciably). Since the KdV soliton is given by

$$\eta = A_0 \operatorname{sech}^2\left[\left(\frac{\beta A_0}{12\alpha}\right)^{1/2}\left(x - c_0 t - \frac{\beta}{3} A_0 t\right)\right],$$

L_s can be taken as

$$L_s = \left(\frac{12\alpha}{\beta A_0}\right)^{1/2}.$$

Therefore the time T_s at which L reaches the value L_s will be

$$T_s = \frac{L_0 - L_s}{\beta A_0}. \tag{7}$$

Note that the difference between the PBBM and the KdV soliton is negligible in most applications (Eilbeck and McGuire 1977) and is certainly of no importance for this scaling argument.

Figure 12 shows the wave profiles at two successive times for various values of the parameters A, T_1 and T_2 of the initial wave and the arrows indicate the distance for which $L = L_s$ according to (7) [the reference point in the wave has been taken to correspond to that at $t = t_0$ in (5)]. Case (a) corresponds to that of section 4: the front is so steep that the dispersive effects, initially negligible, very soon come into play and solitons develop. For smaller values of the amplitude [case (b)] the time T_s is slightly larger because the steepening develops more slowly. On the other hand, if T_1 is large (=2.5 h) solitons cannot be observed at a distance of 45 km from the strait. In case (c) they will start to form at $x \sim 40$ km while in case (d) both nonlinear and dispersive terms are completely negligible with respect to the linear advective term $c_0\eta_x$ of (4) (they would become important when the wave has traveled for so long that other effects would have to be taken into account). In this last case, therefore, the wave travels without any appreciable change in form.

Formula (7) obviously does not apply in the case of KP waves. However, numerical experiments suggest that the mechanism of soliton formation is substantially the same in two dimensions, the 2-D effects having only the important effect of spreading the energy horizontally, thus determining the features of the solitons at each point. One consequence is that the formation of the solitary waves is delayed because the amplitude (which is now space-varying) that should be used to derive a formula like (7) decreases in time. Nevertheless (7) is still useful for the KP dynamics in that it provides a lower bound for the correct T_s. This can be verified by Fig. 13 where KP-wave profiles taken at $y = 0$ are shown for the same parameter values of Fig. 12. These pictures show what the signal measured at, say, P_3 in the various cases would be. While for case (a) (described in section 4) solitary waves can be clearly observed, in the other extreme case (d) a borelike waveform would be found.

6. Conclusions

The inverse problem of determining an initial depression of the interface inside the Strait of Gibraltar, the evolution of which is in agreement with certain current-meter measurements taken in the Alboran Sea, has been solved with a good degree of accuracy. Such an initial wave is also in agreement with possible internal tides generated by the interaction of the semidiurnal tidal current with the major sill, both as far as its amplitude, width and shape are concerned. The Kadomtsev–Petviashvili equation is the model used to study the free evolution of the wave. Despite several simplifying assumptions (no rotation, constant topography, constant depth of the interface, etc.), the KP equation—that to the best of the author's knowledge has never been used before in numerical simulations for oceanographical problems—appears to be a useful tool to model realistic situations such as that dealt with here. Obviously more primitive equations incorporating all the effects neglected here along with real coasts and topography could certainly give more accurate results, but if one considers the paucity of available data, the use of a relatively simple equation like (3) is well justified. Moreover in solving an inverse problem a more primitive model could turn out to be much more difficult to handle. On the other hand, the same KP equation can be extended to include, if necessary, rotation (Grimshaw 1985) and variations in bottom topography (P. L. F. Liu et al. 1985).

The reason why trains of internal solitary waves are not always found at a given distance from the strait has also been clarified. If the front of the initial internal tidal depression inside the strait is not sufficiently steep and/or its amplitude not sufficiently high, nonlinear effects are too weak to act (in the final stage together

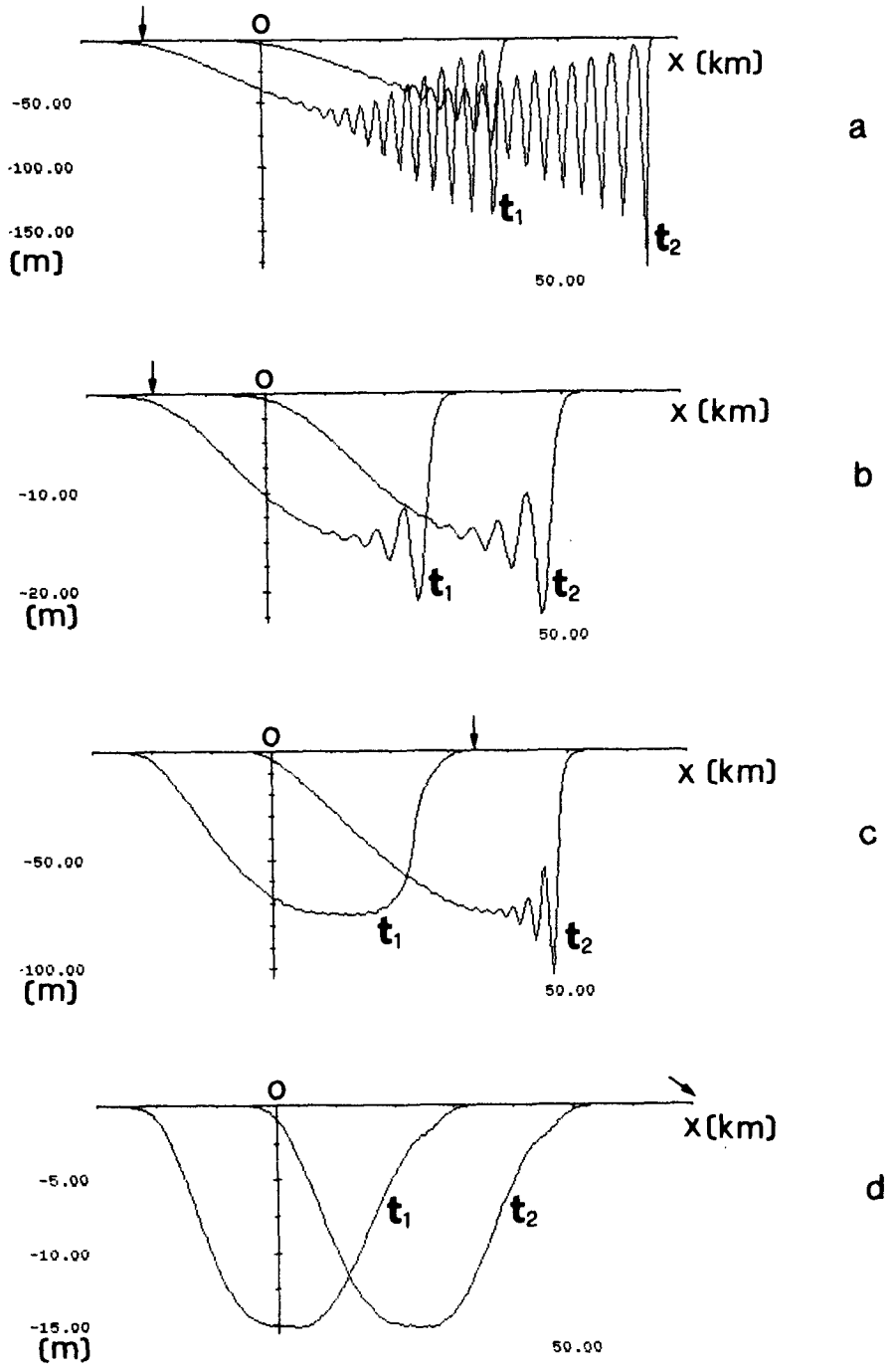

FIG. 12. Wave profiles at t_1 and t_2 obtained by solving the KdV equation for $T_1 = 0.4$ h, $T_2 = 5$ h, $t_0 = 1$ h, $A = -75$ m (a), $T_1 = 0.4$ h, $T_2 = 5$ h, $t_0 = 1$ h, $A = -15$ m (b), $T_1 = 2.5$ h, $T_2 = 2.5$ h, $t_0 = 4.5$ h, $A = -75$ m (c) and $T_1 = 2.5$ h, $T_2 = 2.5$ h, $t_0 = 4.5$ h, $A = -15$ m (d). The arrows indicate the distance at which the leading soliton is expected to be forming according to formula (7).

with dispersion) so as to allow the formation of solitary waves at that distance. However we have not studied why the situation can change from one regime to another. This will be briefly discussed in the remaining part of this section.

As discussed in section 3a, the upstream value of the outflow current determines the kind of depression west of the sill and it is basically given by the sum of the tidal current plus the mean flow. Figure 14 gives an example of such a signal at Tarifa section (see section

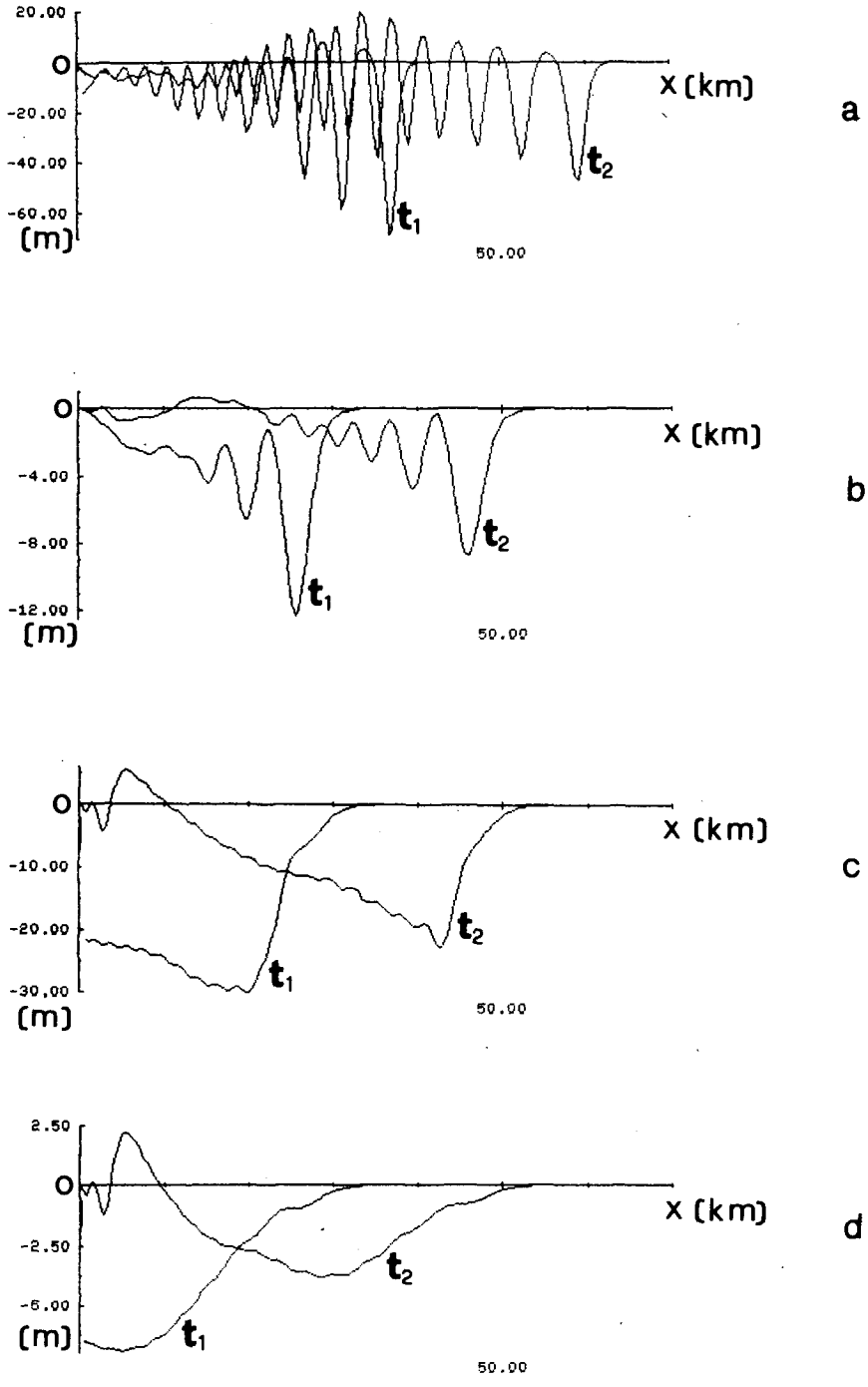

FIG. 13. Wave profiles along the line $y = 0$ obtained by solving the KP equation for the same parameter values of Fig. 12.

3a). As one can see the tidal current has an amplitude of about 1 m s^{-1}, but the outflow component is only about 0.5 m s^{-1} because the oscillation is shifted to the inflow side by the mean Atlantic water inflow. Note that it is the outflow that contributes to the generating mechanism as far as the internal depression eventually propagating into the Alboran Sea is concerned. This implies that, apart from variations related to the spring tidal cycle, fluctuations in the mean flow can have important effects on the character of the internal waves discussed in this paper. On the other hand, low-frequency current fluctuations at the sill with amplitudes of about 40 cm s^{-1} and periods of 15–20 days have indeed been recorded during the recent 1985–86 Gi-

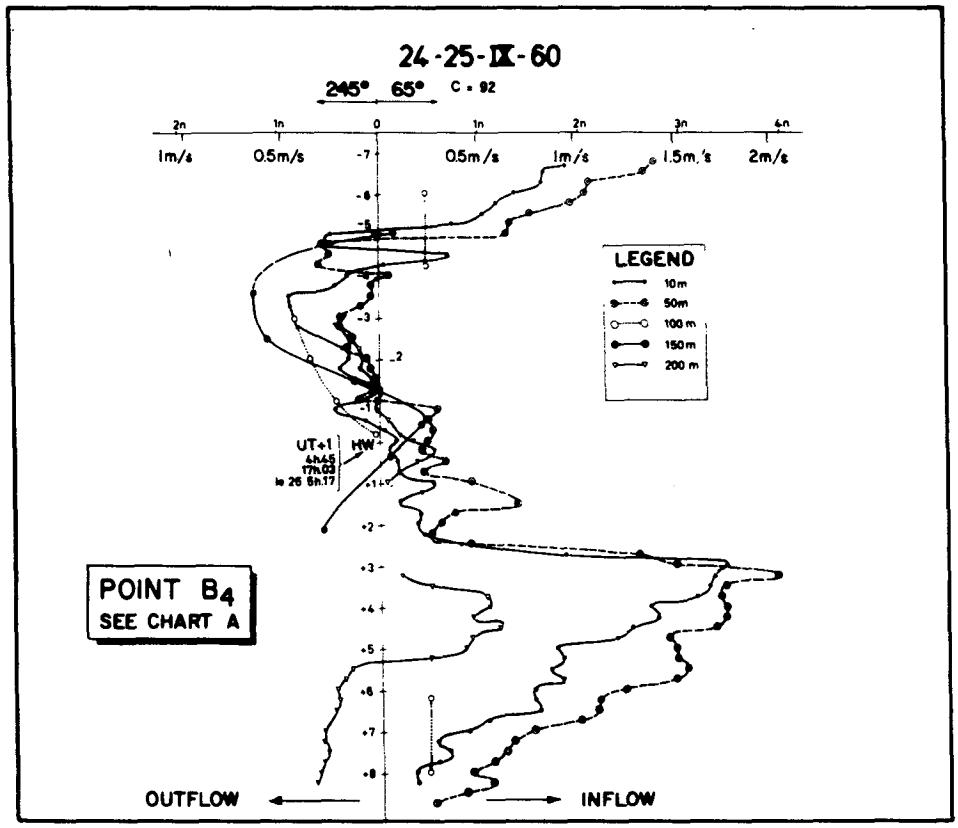

FIG. 14. Example of global along-channel currents measured at about 15 km east of the sill, in Tarifa section (see Fig. 3a). The time in the vertical axis is expressed in hours (after Lacombe and Richez 1982).

braltar Experiment (Kinder and Bryden 1987), although it is not yet clear whether such variations are due to atmospheric pressure or wind stress changes.

The following simple quantitative considerations can help to understand how relevant fluctuations in the mean inflow are to this respect. For typical "upstream" values $H_1 = 150$ m, $H_2 = 350$ m and $b = 200$ m, where b is the height of the sill, the critical Froude number as defined by Long (1954) and already discussed in section 3a is $Fr_c = 0.13$, corresponding to a critical mean flow $U_c \approx 0.4$ m s^{-1} which is comparable to the typical outflow component of the global current, as noticed above. As a consequence one can conjecture that on average the regime is not far from being critical (see Armi and Farmer 1985 for a detailed study on the hydraulics of the mean flow), therefore fluctuations of a few tens of centimeters per second in the mean flow—such as those actually observed—can shift the situation to super or subcritical with a corresponding remarkable effect on the initial internal depression and, therefore, also on the internal wave field in the Alboran Sea (note that in this argument several important effects have not been taken into account, such as the vertical shear of the current and the time variation of the flow). For instance one might pass from a wave packet like that of Fig. 13a to that of Fig. 13d in a few days as a consequence of a weakening of the mean inflow current during this period. This connection had already been suggested by Kinder (1984), who also finds clear experimental evidence. Moreover, he observes a relation between the appearance of packets of strong internal solitary waves in the Alboran Sea and the weakening or even disappearance of the anticyclonic Alboran Sea gyre (La Violette 1984; Parrilla and Kinder 1987). Both effects can be explained as a result of the weakening of the Atlantic water jet, the first on the basis of the aforementioned arguments, the second because it has been shown that the anticyclonic circulation in the western part of the Alboran Sea is substantially forced by the flow entering the sea (Preller 1986).

These considerations show that the understanding of the dynamics of low frequency phenomena in the Western Mediterranean Sea can help explain the formation mechanism of high frequency phenomena such as the Alboran Sea internal solitary waves.

Acknowledgments. I should like to thank T. H. Kinder for having kindly provided CTD time series data and current measurements from the Strait of Gibraltar and the Alboran Sea. In particular the unpublished data in Fig. 11a have made it possible to test the

spreading effects modeled by Eq. (4). This work was supported by FORMEZ (Centro di Formazione e Studi per il Mezzogiorno, Italy) and was carried out at the Center for Meteorology and Physical Oceanography of the Massachusetts Institute of Technology, the use of whose facilities is gratefully acknowledged.

REFERENCES

Alpers, W., and E. Salusti, 1983: Scylla and Charybdis observed from space. *J. Geophys. Res.*, **88,** 1800–1808.

Apel, J. R., J. R. Holbrook, A. K. Liu and J. J. Tsai, 1985: The Sulu Sea internal soliton experiment. *J. Phys. Oceanogr.*, **15,** 1625–1651.

Armi, L., and D. Farmer, 1985: The internal hydraulics of the Strait of Gibraltar and associated sills and narrows. *Oceanol. Acta,* **8,** 37–46.

Benjamin, T. B., 1966: Internal waves of finite amplitude and permanent form. *J. Fluid Mech.*, **25,** 241–270.

——, 1967: Internal waves of permanent form in fluids of great depth. *J. Fluid Mech.*, **29,** 559–592.

——, J. L. Bona and J. J. Mahony, 1972: Model equations for long waves in nonlinear dispersive systems. *Phil. Trans. Roy. Soc. London,* **272A,** 47–78.

Bona, J. L., and R. Smith, 1975: The initial-value problem for the Korteweg-de Vries equation. *Phil. Trans. Roy. Soc. London,* **278A,** 555–604.

Boyce, F. M., 1975: Internal waves in the Strait of Gibraltar. *Deep-Sea Res.*, **22,** 597–610.

David, D., D. Levi and P. Winternitz, 1987: Integrable nonlinear equations for water waves in straits of varying depth and width. *Stud. Appl. Math.*, **76,** 133–168.

Dodd, R. K., J. C. Eilbeck, J. D. Gibbon and H. C. Morris, 1982: *Solitons and Nonlinear Wave Equations.* Academic Press, 630 pp.

Eilbeck, J. C., and G. R. McGuire, 1977: Numerical study of the regularized long-wave equation. Part II: Interaction of solitary waves. *J. Comput. Phys.*, **23,** 63–73.

Farmer, D. M., and D. Smith, 1980: Tidal interaction of stratified flow with a sill in Knight Inlet. *Deep-Sea Res.*, **27,** 239–254.

Frassetto, R., 1964: Short period vertical displacements of the upper layer of the Strait of Gibraltar. SACLANT ASW Centre, La Spezia, No. 30, 49 pp.

Fu, L. L., and B. Holt, 1984: Internal waves in the Gulf of California: observations from a spaceborne radar. *J. Geophys. Res.*, **89,** 2053–2060.

Grimshaw, R., 1985: Evolution equations for weakly nonlinear, long internal waves in a rotating fluid. *Stud. Appl. Math.*, **73,** 1–33.

Haury, L. R., M. G. Briscoe and M. H. Orr, 1979: Tidally generated internal wave packets in Massachusetts Bay. *Nature,* **278,** 312–317.

Hibiya, T., 1986: Generation mechanism of internal waves by tidal flow over a sill. *J. Geophys. Res.*, **91,** 7697–7708.

Joseph, R. I., 1977: Solitary waves in a finite depth fluid. *J. Phys. A: Math. Gen.*, **10,** L225–L227.

Kadomtsev, B. B., and V. I. Petviashvili, 1970: On the stability of solitary waves in weakly dispersing media. *Soviet Phys. Dokl.*, **15,** 539–541.

Katsis, C., and T. R. Akylas, 1987: Solitary internal waves in a rotating channel: a numerical study. *Phys. Fluids,* **30,** 297–301.

Kinder, T. H., 1984: Net mass transport by internal waves near the Strait of Gibraltar. *Geophys. Res. Lett.*, 987–990.

——, and H. L. Bryden, 1987: The 1985–1986 Gibraltar Experiment: data collection and preliminary results. *Eos, Trans. Amer. Geophys. Union,* **68,** No. 40, 786–795.

Koop, C. G., and G. Butler, 1981: An investigation of internal solitary waves in a two-fluid system. *J. Fluid Mech.*, **112,** 225–251.

Korteweg, D. J., and G. de Vries, 1895: On the change of form of long waves advancing in a rectangular canal, and on a new type of long stationary waves. *Phil. Mag.*, **39,** 422–443.

Kubota, T., D. R. S. Ko and D. L. D. Dobbs, 1978: Propagation of weakly nonlinear internal waves in a stratified fluid of finite depth. *A.I.A.A. J. Hydronautics,* **12,** 157–165.

Lacombe, H., and C. Richez, 1982: The regime of the Strait of Gibraltar. *Hydrodynamics of Semi-Enclosed Seas,* J. C. J. Nihoul, Ed., Elsevier, 13–73.

La Violette, P. E., 1984: The advection of submesoscale thermal features in the Alboran Sea gyre. *J. Phys. Oceanogr.*, **14,** 550–565.

Lee, C. Y., and R. C. Beardsley, 1974: The generation of long nonlinear internal waves in a weakly stratified shear flow. *J. Geophys. Res.*, **79,** 453–462.

Liu, A. K., 1983: Detection of bottom features on Seasat Synthetic Aperture Radar imagery. Dynamics Technology Report DT-8312-01, Torrance, CA, 45 pp.

——, J. R. Holbrook and J. R. Apel, 1985: Nonlinear internal wave evolution in the Sulu Sea. *J. Phys. Oceanogr.*, **15,** 1613–1624.

Liu, P. L. F., S. B. Yoon and J. T. Kirby, 1985: Nonlinear refraction-diffraction of waves in shallow water. *J. Fluid Mech.*, **153,** 185–201.

Long, R. R., 1954: Some aspects of the flow of stratified fluids. Part II: Experiments with a two-fluid system. *Tellus,* **6,** 97–115.

Maxworthy, T., 1979: A note on the internal solitary waves produced by tidal flow over a three-dimensional ridge. *J. Geophys. Res.*, **84,** 338–346.

Miles, J. W., 1979: On the Korteweg–de Vries equation for a gradually varying channel. *J. Fluid Mech.*, **91,** 181–190.

Ono, H., 1975: Algebraic solitary waves in stratified fluids. *J. Phys. Soc. Jpn.*, **39,** 1082–1091.

Osborne, A. R., and T. L. Burch, 1980: Internal solitons in the Andaman Sea. *Science,* **208,** 451–460.

Parrilla, G., and T. H. Kinder, 1987: The physical oceanography of the Alboran Sea. NORDA Rep. 184, 26 pp.

Peregrine, D. H., 1966: Calculations of the development of an undular bore. *J. Fluid Mech.*, **25,** 321–330.

Pierini, S., 1986: Solitons in a channel emerging from a three-dimensional initial wave. *Nuovo Cimento,* **9C,** 1045–1061.

Pratt, L. J., 1983: On inertial flow over topography. Part 1: Semi-geostrophic adjustment to an obstacle. *J. Fluid Mech.*, **131,** 195–218.

Preller, R. H., 1986: A numerical model study of the Alboran Sea gyre. *Progress in Oceanography,* vol. 16, Pergamon, 113–146.

Renouard, D. P., G. Chabert d'Hières, and X. Zhang, 1987: An experimental study of strongly nonlinear waves in a rotating system. *J. Fluid Mech.*, **177,** 381–394.

Segur, H., and J. L. Hammack, 1982: Soliton models of long internal waves. *J. Fluid Mech.*, **118,** 285–304.

Tung, K. K., D. R. S. Ko and J. J. Chang, 1981: Weakly nonlinear internal waves in shear. *Stud. Appl. Math.*, **65,** 189–221.